Optical coherent current control at surfaces: Theory of injection current

J. L. Cabellos,[1] Bernardo S. Mendoza,[1] and A. I. Shkrebtii[1,2]
[1]*Division of Photonics, Centro de Investigaciones en Optica, León, Guanajuato, México*
[2]*University of Ontario Institute of Technology 2000 Simcoe Street North, Oshawa, Ontario, Canada L1H 7L7*
(Received 12 September 2011; published 28 November 2011)

We present a study of optical coherent control of injection currents at surfaces of cubic semiconductors, predicting that this new optical effect will serve as a surface-sensitive probe of fundamentally and technologically important crystals with both bulk inversion symmetry (such as cubic diamond $\bar{6}m2$ or $\bar{6}$) and noncentrosymmetric systems (such as zinc-blende symmetry $\bar{4}\bar{3}m$). In crystals with any of these symmetries, this effect vanishes in the bulk, but it is allowed in surface regions due to the breaking of the bulk symmetry there. We present the results of *ab initio* calculations for injected currents at prototypical clean and Sb-covered GaAs(110)(1×1) and clean Si(111)(2×1) surfaces, which have well-understood and experimentally reproducible reconstructions. The effects are shown to be essentially sensitive to surface structure, and the injected currents can be interpreted in terms of the surface electronic structure. Calculated magnitudes indicate that the currents should be easily observable, and the calculated spectra of all of the surfaces demonstrate interesting behavior as a function of the energy of the incident light. Finally, layer-by-layer analysis provide detailed access to the surface properties through explicit separation of the contributions coming from different layers.

DOI: 10.1103/PhysRevB.84.195326 PACS number(s): 78.68.+m, 78.56.−a, 72.40.+w, 42.65.An

I. INTRODUCTION

The understanding and control of structure and chemistry at surfaces is of fundamental and technological importance. Optical probes are of particular interest because they do not require a high vacuum environment, and experiments can be performed at interfaces as well where other techniques are impossible to use. However, because of the long wavelength of the incident light, surface sensitivity typically only arises when the effect under investigation is absent in the underlying bulk or can be compensated using special experimental settings. Two well-known and important examples are reflectance anisotropy spectroscopy (RAS)[1,2] and surface second harmonic generation (SSHG).[3,4] Both have been extensively employed as accurate and noninvasive passive probes of clean and adsorbate-covered surfaces. However, RAS or SHG, crucial for understanding surfaces and interfaces, are not sensitive or cannot be applied to many important systems: RAS is not sensitive to, e.g., optically isotropic Si(111), while SHG signal for III–V or II–VI cubic compounds is influenced by nonzero bulk contribution. In this article we introduce a new surface-sensitive optical effect that offers the potential for not only the study of surfaces and interfaces but for the control of chemical reactions there. This is based on that part of the optical susceptibility that demonstrates very unusual symmetry properties compared to the above mentioned optical techniques. It relies on the breaking of the bulk symmetry at the surface, such as other surface-sensitive methods. However, within the susceptibility framework of optical response this effect is a nonlinear one since it is proportional to the product of two incoming electric fields [see Eq. (1)]. Its amplitude, however, scales linearly with the incident light intensity, which is proportional to the modulus squared of the amplitude of the fields [see Eq. (17)]. In some excitation scenarios a current can be injected in the surface region by an incident optical field, with a variation in time that is driven by the time dependence of the incident intensity. In pulsed excitation the effect can be detected through the emission of THz radiation, which is caused by acceleration of the charges making up the injected current.[5,6] It can also be studied, in both pulsed and CW excitation setup, by measuring a voltage induced along the surface.[7]

The simplest such phenomenon is *below band-gap* optical rectification, where a polarization current is induced by an optical field at incident frequencies below the energy gap of a semiconductor or insulator; the polarization follows the incident intensity in its time evolution, and its time derivative yields a current that can drive THz radiation. This current, which vanishes for CW radiation, is not our concern here. Rather, we focus on light with incident frequencies *above the band gap*, where not only virtual but real excitations are present. For such incident frequencies there are, generally speaking, two new currents that can be optically excited.[8,9]

The first is a shift current, $\mathbf{J}_{\text{shift}}$, associated with the motion of the center of charge of electrons as they are promoted from valence to conduction bands; to good approximation it is proportional to the pulse intensity.[10] The second is an injection current, $\mathbf{J}_{\text{inj}}$, associated with a polar asymmetry of injected electrons and holes in reciprocal space; to good approximation $d\mathbf{J}_{\text{inj}}/dt$ is proportional to the pulse intensity as well, and the injection can be understood as a quantum interference between absorption events associated with different linear polarizations. In both effects the energy increase of the carriers is provided by the electromagnetic field, while the increase in momentum is provided by the crystal lattice. In the bulk of crystals without inversion symmetry the injection and shift currents fall into the phenomenological categories of a circular photogalvanic effect and a linear photogalvanic effect, respectively,[11] and their description has been formulated in the context of nonlinear optics.[8,9,12,13] As shorter and shorter pulses are considered, the distinction between these terms (and optical rectification, which still exists above the band gap) becomes less sharp. Nonetheless, in the CW limit the injection current in a bulk medium is characterized by a third rank tensor η^{abc},

$$j^a_{\text{inj}} = 2\eta^{abc}_{\text{bulk}}(0;\omega,-\omega)E^b(\omega)E^c(-\omega), \tag{1}$$

where the superscripts indicate Cartesian components that are to be summed over if repeated, and $E^a(\omega)$ indicates the electric field along the "a" axis at the incident frequency ω; in the independent particle approximation the coefficient η^{abc}_{bulk} is antisymmetric in the components b and c and purely imaginary.[8,9] For slowly varying pulses the intensity-like term $E^b(\omega)E^c(-\omega)$ can be multiplied by a function describing the time dependence of the intensity in the pulse,[8] and the resulting equation can be used to determine the injected current in the absence of scattering and space charge effects. The tensor η^{abc}_{bulk} gives the injected current along direction "a" induced by two electric fields along directions "b" and "c," respectively. These fields must be perpendicular to each other due to the fact that the tensor is antisymmetric on b and c indices, and, in general, these fields are phase shifted such as that of circularly polarized light. This phase shift allows the coherent control of the injected current [see Eq. (17)].

In this paper we focus on the injection current that, being forbidden in the bulk, becomes allowed at surfaces of crystals or interfaces. This includes not only centrosymmetric crystals (such as Si) but also the crystal classes $\bar{6}m2$, $\bar{6}$, and $\bar{4}\bar{3}m$, the last of which includes typical III–V semiconductors such as GaAs. We note that the different effects, mentioned above, can be distinguished from each other by their dependence on pulse width and from phase-insensitive photovoltaic effects by their dependence on the polarization of the incident field.[8,14] We feel that current injection is the most striking of these as-yet-uninvestigated surface processes, since it vanishes in the bulk in many semiconductors of both fundamental and applied interest, thus reflecting purely surface properties. Furthermore, the injection current would give an experimentalist the opportunity to "shoot" electrons and holes in one or another direction along the surface, which is particularly exciting.

At a surface of the above semiconductors, Eq. (1) can be replaced by a corresponding equation involving the surface injection current $\dot{\mathbf{J}}^S_{\text{inj}}$ (here S stands for surface) and a surface response coefficient $\eta^{S,abc}$. We evaluate $\eta^{S,abc}$ for the well-studied Si(111) 2×1 reconstructed surface[15,16] and two of the GaAs(110) surfaces;[17] the results demonstrate that the injection current is sensitive to the fine details of surface structure and the type of chemical bonding. Furthermore, we show that it can be understood in a simple way in terms of the properties of electronic surface states, and it should be amenable to experimental study.

The article is organized as follows. In Sec. II we present the formalism for the surface-injected current, based on an approach that is well suited for a surface calculation. Then, in Sec. III we present the computational details of the *ab initio* method used in our calculations, and in Sec. IV we discuss the results for the surfaces under consideration. Finally, the conclusions are given in Sec. V.

II. THEORY

In this section we derive the expressions for the generation rate of the injection current suitable for surfaces and interfaces. We model the semi-infinite crystal using a slab consisting of N atomic layers inside a supercell of total height L and volume $\Omega = AL$, where A is the area of the surface unit cell. The supercell includes a L_v-thick vacuum region required to use a repeated slab scheme,[18] thus, $L = L_s + L_v$, where L_s is the semiconductor slab thickness. In a slab calculation, it is often important and instructive to calculate the response from a particular layer of the slab. A convenient way to accomplish the separation of the response of any layer is to introduce the so called "cut function," $\mathcal{F}_\ell(z)$, as a top-hat cut function that selects a given layer,

$$\mathcal{F}_\ell(z) = \Theta\left(z - z_\ell + \Delta^b_\ell\right)\Theta\left(z_\ell - z + \Delta^f_\ell\right), \tag{2}$$

where Θ is the Heaviside function. Here, $\Delta^{f/b}_\ell$ is the distance that the ℓ-th layer extends toward the front (f) or back (b) from its z_ℓ position. Thus, $\Delta^f_\ell + \Delta^b_\ell$ is the thickness of layer ℓ. Such a function was originally used by Hogan *et al.*[19] and Castillo *et al.*,[20] and more recently was put on a more solid basis through a microscopic calculation of the linear optical response of surfaces by Mendoza *et al.*[21] The above scheme known as a layer-by-layer formalism was successfully used to provide deeper and optional understanding of various surface optical responses, calculated initially for the whole slab.[19–22] For this work, however, the use of the layer-by-layer approach is mandatory since without layer-by-layer separation it is impossible to perform a physically relevant calculation for the surface injection current using slab method.

To derive an expression for the rate of change of the injection current, suitable for a surface, we follow a Fermi's golden rule (FGR) approach. We have to stress that for a bulk calculation one may use the formalism of Ref. 9 based on the usual approach for nonlinear optics. However, the FGR gives a simpler and more insightful derivation of the *surface* injection current. We use the independent particle approximation and, as it is usually done for numerically expensive simulations, neglect local field and excitonic effects and treat the electromagnetic field classically, while the electrons in semiconductor slabs are treated quantum-mechanically. The current density operator is written as

$$\hat{j}^a(\mathbf{r}) = \sum_{mn\mathbf{k}} j^a_{nm}(\mathbf{r};\mathbf{k})\hat{c}^\dagger_{n\mathbf{k}}\hat{c}_{m\mathbf{k}}. \tag{3}$$

Here $\hat{c}^\dagger_{n\mathbf{k}}$ ($\hat{c}_{n\mathbf{k}}$) creates (annihilates) an electron in a Bloch state $|n\mathbf{k}\rangle$, labeled by a band index n and crystal momentum $\mathbf{k}$, and

$$j^a_{nm}(\mathbf{r};\mathbf{k}) = \frac{-i\hbar}{2m_e}\left[\psi^*_{n\mathbf{k}}(\mathbf{r})\frac{\partial}{\partial r^a}\psi_{m\mathbf{k}}(\mathbf{r}) - \psi_{m\mathbf{k}}(\mathbf{r})\frac{\partial}{\partial r^a}\psi^*_{n\mathbf{k}}(\mathbf{r})\right] \tag{4}$$

are the matrix elements of the current operator, where $\psi_{n\mathbf{k}}(\mathbf{r}) = \langle\mathbf{r}|n\mathbf{k}\rangle$ is the coordinate representation of the ket $|n\mathbf{k}\rangle$ and m_e is the mass of the electron. To move into an electron-hole picture, we introduce electron ($\hat{a}^\dagger$,$\hat{a}$) and hole ($\hat{b}^\dagger$,$\hat{b}$) operators in the usual way through the transformations

$$\hat{c}^\dagger_{n\mathbf{k}} = \hat{a}^\dagger_{c\mathbf{k}}\delta_{nc} + \hat{b}_{v\mathbf{k}}\delta_{nv},$$

and

$$\hat{c}_{n\mathbf{k}} = \hat{a}_{c\mathbf{k}}\delta_{nc} + \hat{b}^\dagger_{v\mathbf{k}}\delta_{nv},$$

where δ_{nc} (δ_{nv}) is one if n is a conduction (valence) band $c(v)$ and zero otherwise. In the electron-hole picture, Eq. (3) becomes

$$\hat{j}^a(\mathbf{r}) = \sum_{cc'\mathbf{k}} j^a_{cc'}(\mathbf{r};\mathbf{k})\hat{a}^\dagger_{c\mathbf{k}}\hat{a}_{c'\mathbf{k}} + \sum_{vv'\mathbf{k}} j^a_{vv'}(\mathbf{r};\mathbf{k})\hat{b}_{v\mathbf{k}}\hat{b}^\dagger_{v'\mathbf{k}} + \sum_{cv\mathbf{k}} j^a_{cv}(\mathbf{r};\mathbf{k})\hat{a}^\dagger_{c\mathbf{k}}\hat{b}^\dagger_{v\mathbf{k}} + \sum_{cv\mathbf{k}} j^a_{vc}(\mathbf{r};\mathbf{k})\hat{a}_{c\mathbf{k}}\hat{b}_{v\mathbf{k}},$$

from where one can show that for the ground-state $\langle 0|\hat{j}^a(\mathbf{r})|0\rangle = 0$, and for an arbitrary electron-hole state, $|cv\mathbf{k}\rangle$,

$$\langle cv\mathbf{k}|\hat{j}^a(\mathbf{r})|cv\mathbf{k}\rangle = j^a_{cc}(\mathbf{r};\mathbf{k}) - j^a_{vv}(\mathbf{r};\mathbf{k}),$$

where we used the anticommutator relationships $\{\hat{a}_{c\mathbf{k}},\hat{a}^\dagger_{c'\mathbf{k}}\} = \delta_{cc'}$ and $\{\hat{b}_{v\mathbf{k}},\hat{b}^\dagger_{v'\mathbf{k}}\} = \delta_{vv'}$, with the anticommutator of all other combinations of operators equal to zero.

In order to calculate the expectation value of the injected current,

$$\langle j^a(\mathbf{r})\rangle = \langle\phi(t)|\hat{j}^a(\mathbf{r})|\phi(t)\rangle, \tag{5}$$

we expand the time-dependent wavefunction as

$$|\phi(t)\rangle = C_0(t)|0\rangle + \sum_{vc\mathbf{k}} C_{cv\mathbf{k}}(t)|cv\mathbf{k}\rangle$$

and use standard quantum mechanical perturbation theory to find that the FGR gives

$$\frac{d}{dt}|C_{cv\mathbf{k}}(t)|^2 = 2\pi\,|V_{cv\mathbf{k}}|^2\delta(\omega_{cv}(\mathbf{k}) - \omega),$$

with

$$V_{cv\mathbf{k}} = -\frac{e}{\hbar}\mathbf{r}_{cv}(\mathbf{k})\cdot\mathbf{E}(\omega),$$

where we have used $-e\mathbf{r}\cdot\mathbf{E}(t)$ as perturbation with $\mathbf{r}$ the position operator of the electron of charge e, with $\mathbf{r}_{nm}(\mathbf{k})$ its matrix elements, and $\mathbf{E}(t)$ the incoming monochromatic electric field written as $\mathbf{E}(t) = \mathbf{E}(\omega)e^{-i(\omega-i\eta)t} + \text{c.c.}$ The parameter $\eta > 0$ is used to turn on the perturbation adiabatically and the limit of $\eta \to 0$ was taken at the end of the calculation. Also, we assumed the long wavelength approximation for the incoming field. Using Eq. (5) we get that the rate of change of the macroscopic injection current, $\mathbf{J}_{\text{inj}}(\mathbf{r})$, is given by

$$\begin{aligned} j^a_{\text{inj}}(\mathbf{r}) &= e\frac{d}{dt}\langle j^a(\mathbf{r})\rangle \\ &= 2\pi\Omega\int\frac{d^3k}{8\pi^3} \\ &\quad\times\sum_{vc}|V_{cv\mathbf{k}}|^2 e\big[j^a_{cc}(\mathbf{r};\mathbf{k}) - j^a_{vv}(\mathbf{r};\mathbf{k})\big]\delta[\omega_{cv}(\mathbf{k}) - \omega], \end{aligned}$$

where we used the fact that in the continuous limit of $\mathbf{k}$, $\sum_{\mathbf{k}} \to \Omega\int d\mathbf{k}/(8\pi^3)$, with Ω the unit cell volume. The above equation gives the rate of change of the injection current as a function of $\mathbf{r}$. In terms of a response function we follow Ref. 9 to write

$$\begin{aligned} j^a_{\text{inj}}(\mathbf{r}) &= \eta^{abc}(\mathbf{r}|0;\omega,-\omega)E^b(\omega)E^c(-\omega) \\ &\quad + \eta^{abc}(\mathbf{r}|0;-\omega,\omega)E^b(-\omega)E^c(\omega) \\ &= \eta^{abc}(\mathbf{r}|0;\omega,-\omega)E^b(\omega)E^c(-\omega) + \text{c.c.} \\ &= 2\eta^{abc}(\mathbf{r}|0;\omega,-\omega)E^b(\omega)E^c(-\omega), \end{aligned} \tag{6}$$

where $\mathbf{E}(-\omega) = \mathbf{E}^*(\omega)$ and

$$\eta^{abc}(\mathbf{r}|0;\omega,-\omega) = \frac{\pi e^3}{\hbar^2}\Omega\int\frac{d^3k}{8\pi^3}\sum_{vc}\Delta^a_{cv}(\mathbf{r};\mathbf{k})r^b_{cv}(\mathbf{k})r^c_{vc}(\mathbf{k}) \times\delta[\omega_{cv}(\mathbf{k}) - \omega]. \tag{7}$$

We defined

$$\Delta^a_{cv}(\mathbf{r};\mathbf{k}) \equiv j^a_{cc}(\mathbf{r};\mathbf{k}) - j^a_{vv}(\mathbf{r};\mathbf{k})$$

and used the hermiticity of $\mathbf{r}_{nm}(\mathbf{k}) = \mathbf{r}^*_{mn}(\mathbf{k})$. Using time-reversal symmetry, $\mathbf{r}_{nm}(-\mathbf{k}) = \mathbf{r}_{mn}(\mathbf{k})$ and $\mathbf{j}_{nm}(\mathbf{r};-\mathbf{k}) = -\mathbf{j}_{mn}(\mathbf{r};\mathbf{k})$, we can rewrite Eq. (7) as

$$\begin{aligned} \eta^{abc}(\mathbf{r}|0;\omega,-\omega) &= \frac{i\pi e^3}{\hbar^2}\Omega\int\frac{d^3k}{8\pi^3}\sum_{vc}\Delta^a_{cv}(\mathbf{r};\mathbf{k})\text{Im} \\ &\quad\times\big[r^b_{cv}(\mathbf{k})r^c_{vc}(\mathbf{k})\big]\delta[\omega_{cv}(\mathbf{k}) - \omega] \\ &= \frac{\pi e^3}{2\hbar^2}\Omega\int\frac{d^3k}{8\pi^3}\sum_{vc}\Delta^a_{cv}(\mathbf{r};\mathbf{k}) \\ &\quad\times\big[r^b_{cv}(\mathbf{k}),r^c_{vc}(\mathbf{k})\big]\delta[\omega_{cv}(\mathbf{k}) - \omega], \end{aligned} \tag{8}$$

where we obtain that the tensor $\eta^{abc}(\mathbf{r}|0;\omega,-\omega)$, which gives the rate of injection current at observation point $\mathbf{r}$ through Eq. (6), is purely imaginary and it satisfies, among other relations, $\eta^{abc}(\mathbf{r}|0;\omega,-\omega) = -\eta^{acb}(\mathbf{r}|0;\omega,-\omega) = -[\eta^{abc}(\mathbf{r}|0;\omega,-\omega)]^*$. These relations were used in the derivation of Eq. (6).

In the case of surfaces, using Eq. (2) we define the contribution to the injected current density from the ℓ-th layer of the slab as

$$\begin{aligned} j^a_{\text{inj}}(\ell) &\equiv \frac{1}{\Omega}\int d\mathbf{r}\mathcal{F}_\ell(z)j^a_{\text{inj}}(\mathbf{r}) \\ &= \frac{1}{\Omega}\int d\mathbf{r}\mathcal{F}_\ell(z)\eta^{abc}(\mathbf{r}|0;\omega,-\omega)E^b(\omega)E^c(-\omega) \\ &\equiv \eta^{abc}(\ell|0;\omega,-\omega)E^b(\omega)E^c(-\omega), \end{aligned} \tag{9}$$

where

$$\eta^{abc}(\ell|0;\omega,-\omega) = \frac{i\pi e^3}{\hbar^2}\int\frac{d^3k}{8\pi^3}\sum_{vc}\Delta^a_{cv}(\ell;\mathbf{k})\text{Im} \times\big[r^b_{cv}(\mathbf{k})r^c_{vc}(\mathbf{k})\big]\delta[\omega_{cv}(\mathbf{k}) - \omega], \tag{10}$$

with

$$\Delta^a_{cv}(\ell;\mathbf{k}) = \int d\mathbf{r}\mathcal{F}_\ell(z)\Delta^a_{cv}(\mathbf{r};\mathbf{k}). \tag{11}$$

The above integral involves the integration of $j^a_{nm}(\mathbf{r};\mathbf{k})$, which from Eq. (4) gives

$$\begin{aligned} &\int d\mathbf{r}\mathcal{F}_\ell(z)j^a_{nm}(\mathbf{r};\mathbf{k}) \\ &= \frac{-i\hbar}{2m_e}\int d\mathbf{r}\mathcal{F}_\ell(z)\left[\psi^*_{n\mathbf{k}}(\mathbf{r})\frac{\partial}{\partial r^a}\psi_{m\mathbf{k}}(\mathbf{r}) - \psi_{m\mathbf{k}}(\mathbf{r})\frac{\partial}{\partial r^a}\psi^*_{n\mathbf{k}}(\mathbf{r})\right] \\ &= \frac{1}{m_e}\int d\mathbf{r}\psi^*_{n\mathbf{k}}(\mathbf{r})\left[\frac{\mathcal{F}_\ell(z)\hat{p}^a + \hat{p}^a\mathcal{F}_\ell(z)}{2}\right]\psi_{m\mathbf{k}}(\mathbf{r}) \\ &= \frac{1}{m_e}\int d\mathbf{r}\psi^*_{n\mathbf{k}}(\mathbf{r})\hat{\mathcal{P}}^a_\ell(z)\psi_{m\mathbf{k}}(\mathbf{r}) \\ &\equiv \frac{1}{m_e}\mathcal{P}^a_{nm}(\ell\mathbf{k}), \end{aligned}$$

where we integrated by parts the second term in the right-hand side of the above equation, wrote $\hat{p}^a$ for $-i\hbar\partial/\partial r^a$, and defined

$$\hat{\mathcal{P}}^a_\ell(z) = \tfrac{1}{2}[\mathcal{F}_\ell(z)\hat{p}^a + \hat{p}^a\mathcal{F}_\ell(z)],$$

which is the momentum operator suitable for a "layer-by-layer" calculation.[21] If we take $\mathcal{F}_\ell(z) = 1$ throughout the supercell, $\mathcal{P}^a_{nm}(\ell;\mathbf{k}) \to p^a_{nm}(\mathbf{k})$, and Eq. (11) leads to $\Delta^a_{cv}(\ell;\mathbf{k}) \to \Delta^a_{cv}(\mathbf{k}) = v^a_{cc}(\mathbf{k}) - v^a_{vv}(\mathbf{k})$, with $v^a_{nn}(\mathbf{k}) = p^a_{nn}(\mathbf{k})/m_e$ the electron's velocity for band n. In turn, $\eta^{abc}(\ell|0;\omega,-\omega) \to \eta^{abc}_{\rm bulk}(0;\omega,-\omega)$, which from the second line of Eq. (8) leads to the same result as that of Eq. (55) of Ref. 9 derived for a bulk system from a nonlinear optics approach. Finally, Eq. (11) reduces to

$$\Delta^a_{cv}(\ell;\mathbf{k}) = \mathcal{V}^a_{cc}(\ell;\mathbf{k}) - \mathcal{V}^a_{vv}(\ell;\mathbf{k}), \tag{12}$$

where $\mathcal{V}^a_{nn}(\ell;\mathbf{k}) = \mathcal{P}^a_{nn}(\ell;\mathbf{k})/m_e$ is the electron's velocity along the Cartesian direction "a" for the n-th energy band and the ℓ-th layer. With Eq. (12), $\eta^{abc}(\ell|0;\omega,-\omega)$ of Eq. (10) can be readily calculated. An explicit expression for $\mathcal{V}^a_{nn}(\ell;\mathbf{k})$ in terms of plane waves is given in Ref. 21.

Before we proceed, some words of caution are required. The electric field of Eq. (6) is implicitly taken as uniform in the region of interest, i.e., Eq. (9). Clearly this is inappropriate for the normal to the surface z component of the electric field, which for semiconductors can change by orders of magnitude as one moves from vacuum to within the semiconductor. Thus, all aspects of the optical response at an interface due to this component of the electric field would require a self-consistent calculation of the variation of E^z across the surface region.[23] Although the calculation of this variation is an important issue, we do not address it here. Instead, we focus on the commonly used experimental geometry of normal incidence. Then the electric field vectors are in the plane of the interface xy, and they can be taken as uniform through the interface region, by neglecting the local field corrections that is typically done even in many less numerically consuming bulk calculations. Also, any calculation of the z component of the injection current density, regardless of what fields are involved, would have to be handeled with care, since injection current in the z direction would at a real surface correspond to a directed photoionization effect, and that of course cannot be dealt with correctly in a supercell calculation such as ours.

To perform the integral over the Brillouin zone (BZ), as required by Eq. (10), we follow Ref. 24 and use only k points in an irreducible "wedge" of the BZ. At any k point outside a specified irreducible wedge, the matrix elements $r^a_{nm}(\mathbf{k})$ and $\mathcal{V}^a_{nm}(\ell,\mathbf{k})$ can be determined from the matrix elements at an equivalent point inside the irreducible wedge via the point group operation relating the two k points. Indeed, for each point group symmetry operation, characterized by a 3×3 matrix $\boldsymbol{\alpha}_s$, the following relations are satisfied: $r^a_{nm}(\boldsymbol{\alpha}\mathbf{k}) = \alpha^{ab}r^b_{nm}(\mathbf{k})$, $\mathcal{V}^a_{nm}(\ell,\boldsymbol{\alpha}\mathbf{k}) = \alpha^{ab}\mathcal{V}^b_{nm}(\ell,\mathbf{k})$, and $\omega_n(\boldsymbol{\alpha}\mathbf{k}) = \omega_n(\mathbf{k})$. To calculate any given tensor component of Eq. (10), we use a scalar representation and thus the integrand transforms throughout reciprocal space as a scalar, and so the integral over any irreducible wedge gives the same result. Each tensor component is invariant under the point group symmetry operations, and the scalar representation gives

$$\eta^{ijk}(\ell|0;\omega,-\omega) = \frac{1}{\mathcal{N}_{\rm sym}}\sum_{s=1}^{\mathcal{N}_{\rm sym}}\alpha^{ia}_s\alpha^{jb}_s\alpha^{kc}_s\eta^{abc}(\ell|0;\omega,-\omega), \tag{13}$$

which more accurately reflects how we compute the response, with $\mathcal{N}_{\rm sym}$ the number of point group operations in the BZ. From Eq. (10) this gives

$$\eta^{ijk}(\ell|0;\omega,-\omega) = \frac{i\pi e^3}{\hbar^2\mathcal{N}_{\rm sym}}\int_w\frac{d^3k}{8\pi^3}\sum_{vc}\sum_{s=1}^{\mathcal{N}_{\rm sym}}\alpha^{ia}_s\alpha^{jb}_s\alpha^{kc}_s\Delta^a_{cv} \times(\ell;\mathbf{k})\mathrm{Im}\big[r^b_{cv}(\mathbf{k})r^c_{vc}(\mathbf{k})\big]\delta(\omega_{cv}(\mathbf{k})-\omega), \tag{14}$$

where the subscript w on the integral symbol indicates that the integral should be done over an irreducible wedge.

The above expression for $\eta^{ijk}(\ell|0;\omega,-\omega)$ is such that for a centrosymmetric system (such as, e.g., Si bulk or a slab with a center of symmetry) it is identically zero, since for such a system the matrix elements r^a_{nm} are real and then the imaginary part term in Eq. (14) would vanish, regardless of the point group symmetry operation $\boldsymbol{\alpha}_s$. However, for noncentrosymmetric systems, such as GaAs and GaAs-based slabs, $\mathrm{Im}[r^b_{cv}(\mathbf{k})r^c_{cv}(\mathbf{k})]$ is in general different from zero, and $\eta^{abc}(\ell|0;\omega,-\omega)$ from Eq. (10) is finite, which is spurious. For these systems the vanishing of $\eta^{ijk}(\ell|0;\omega,-\omega)$ is through their point group symmetry operations as given by Eq. (13). Indeed, as we have mentioned, for noncentrosymmetric bulk GaAs is its crystal class $\bar{4}\bar{3}m$ that has the corresponding point group symmetry operations $\boldsymbol{\alpha}_s$ that render $\eta^{ijk}_{\rm bulk}(0;\omega,-\omega) \equiv 0$.

A. Surface injection current

In order to define the injection current suitable for a surface calculation, we take into account the following observations. As it was mentioned before, the slab that we use to represent the surface of the system consists of N layers. Such slab must be noncentrosymmetric; otherwise, as explained above $\eta^{ijk}(\ell|0;\omega,-\omega) = 0$. As the point group symmetry operations of the slab is different from that of the bulk of the system in question, we should expect a nonvanishing $\eta^{ijk}(\ell|0;\omega,-\omega)$ for every layer of the slab, which is a spurious effect that has to be excluded from the surface-originated signal. To tackle this problem, let us introduce N_c, the minimum number of layers inside the slab at which we can neglect changes of $\eta^{ijk}(\ell|0;\omega,-\omega)$ for different ℓ. If ℓ_B, is the layer number at the middle of the slab, it is reasonable to expect that for layers, $\tilde{\ell}$, close to ℓ_B $\eta^{ijk}(\tilde{\ell}|0;\omega,-\omega) \simeq \eta^{ijk}(\ell_B|0;\omega,-\omega)$. When approaching the layers, close to the surface, deviation of $\eta^{ijk}(\ell|0;\omega,-\omega)$ from its value at ℓ_B is only due to the surface effects. Therefore, we can use $(1/A)\sum_{\ell=1}^{\ell_B}\Omega[\eta^{ijk}(\ell|0;\omega,-\omega) - \eta^{ijk}(\ell_B|0;\omega,-\omega)]$ as a surface response. The validity of such an assumption will be proven when presenting the results of the calculation for GaAs surfaces. The value of L_s should be chosen such that the calculated response converges with respect to the slab thickness and the value of L_v should be large enough to

avoid the interference of the slabs in adjacent unit supercells.[25] L_s includes all the layers of the slab, but those layers close to the center of the slab have to yield zero response, as discussed before. To finally get the expression for the injection current, we introduce an effective thickness $L_{\rm eff}$ of the layers that adds to the surface contribution. If $\ell_{\rm eff}$ is the last layer (counting from the surface) that contributes, we define the surface response as

$$\begin{aligned}\eta^{S,ijk}(0;\omega,-\omega)&\\ &\equiv L_{\rm eff}\sum_{\ell=1}^{\ell_{\rm eff}}[\eta^{ijk}(\ell|0;\omega,-\omega)-\eta^{ijk}(\ell_B|0;\omega,-\omega)]\\ &=\sum_{\ell=1}^{\ell_{\rm eff}}[\tilde{\eta}^{ijk}(\ell|0;\omega,-\omega)-\tilde{\eta}^{ijk}(\ell_B|0;\omega,-\omega)],\end{aligned}\qquad(15)$$

with $\tilde{\eta}^{ijk}(\ell|0;\omega,-\omega)=L_{\rm eff}\eta^{ijk}(\ell|0;\omega,-\omega)$. The next layers that follow $\ell_{\rm eff}$ till ℓ_B can be neglected compared to the total sum. Thus, only the surface layer and the layers close to it will contribute to $\eta^{S,ijk}(0;\omega,-\omega)$. Finally, from Eq. (9) we write

$$j^{S,i}_{\rm inj}=\eta^{S,ijk}(0;\omega,-\omega)E^i(\omega)E^k(-\omega),\qquad(16)$$

as the surface injection current, where both $j^{S,i}_{\rm inj}$ and $\eta^{S,ijk}(0;\omega,-\omega)$ have the units of their bulk counterparts times that of length as they should for a surface response.

III. COMPUTATIONAL DETAILS

The numerical part of our layer-by-layer analysis is performed with the ABINIT plane-wave code based on the density functional theory (DFT) within the local density approximation (LDA).[26] A self-consistent calculation is carried out first to determine the Kohn-Sham potential for the relaxed surface structures. We use the separable Hartwigsen-Goedecker-Hutter (HGH) pseudopotentials[27] within the LDA as parametrized by Goedecker *et al.*[28] In our calculations for Si and GaAs surfaces, we exclude the semicore states, as it is usually done, though they can be included with more computational effort. For optics in Si and GaAs, the core state contribution is negligible. Once the Kohn-Sham potential is determined, we find the wavefunctions, and then the matrix elements are calculated for **k**-points on a specially determined tetrahedral grid. This grid is used in the integrals of Eq. (14), which are conveniently done by a linear analytic tetrahedral integration method.[24] A set of 802 **k**-points in the irreducible surface Brillouin zone (SBZ) and a cut-off energy of 10 Hartree produces converged results for each of the surfaces. The required matrix elements are calculated as proposed in Ref. 21. To correct the DFT LDA energy gap underestimation with respect to the experimental value, the quasiparticle (QP) corrections, such as in Refs. 29–31, have to be included. However, for the very large slabs used in this study it is computationally prohibitive to apply such approaches. On the other hand, the QP corrections could accurately be incorporated at the scissors operator level with great success.[32,33] Therefore, we use such a correction, which for the calculated response only implies the rigid shift of the optical spectra by the scissors correction.[8,34] The interaction term of the Hamiltonian $-e\mathbf{r}\cdot\mathbf{E}$ is in the so-called length gauge. In such a case, care should be taken in order to properly incorporate the scissors correction in systems with periodic boundary conditions such as the supercell used in here. Indeed, one has to properly decompose the position operator **r** into interband and intraband contributions in order to include the scissors operator. This is now a well-defined approach, as in Ref. 8, from where we follow the same procedure. Finally, we have neglected local field and excitonic effects; including any of these is a numerical challenge for the very big slabs that we are using.

As we mentioned above, a noncentrosymmetric slab is required for the calculation; one of its surfaces ("front surface") represents the surface under investigation and has its other surface ("back surface") terminated differently. The "middle" of the slab consists of planes of atoms at their ideal bulk positions. It is common to terminate the back surface with hydrogen, since H atoms can simply saturate the dangling bonds, thus producing a "bulk-like" termination to the slab.[35] However, as the response of the front surface should not depend on the response of the back surface, it is also possible and instructive to terminate the back surface with a different reconstruction. Indeed, for GaAs(110) the front surface of the slab can represent the clean surface, while the back surface can represent the Sb-covered surface. Such a slab not only ensures the absence of centrosymmetric symmetry but also could be used to prove the validity of the layer-by-layer approach for the calculation of the surface injection current.

IV. RESULTS

In this section we present our results using the full-band electronic scheme developed in Sec. II. The chosen examples are the clean and Sb-covered GaAs(110)(1×1) relaxed surfaces and the clean Si(111)(2×1) reconstructed surface (see Fig. 1). We have considered these surfaces since their structures are well understood and are easy to reproduce experimentally. The nonzero (symmetry allowed) components of $\eta^{S,abc}(0;\omega,-\omega)$ for all the surfaces under consideration are the yyx, xzx, and yzy components. The last two components include the electric field perpendicular to the surface, and as discussed above, it requires a detailed calculation of E^z.[23] Therefore, although the injection current should exist for all three components, here we only present results for the first yyx component. The $\eta^{S,yyx}(0;\omega,-\omega)$ tensor component requires a field circularly polarized and parallel to the surface, which corresponds to normal incidence, a setup mostly used in optical experiments. For instance, taking $E^x(\omega)=E_0(\omega)$ and $E^y(\omega)=E_0(\omega)e^{i\phi}$, shifted with respect to the x component by a phase ϕ, one gets from Eq. (16) that

$$j^{S,y}_{\rm inj}=2i\eta^{S,yyx}(0;\omega,-\omega)|E_0(\omega)|^2\sin\phi,\qquad(17)$$

from where it follows that the rate of injected current along y is proportional to the phase difference of the field through a sine dependence.

A. GaAs(110) surfaces

The GaAs surfaces considered here are the clean (110) and Sb-covered (110) surfaces, both (1×1) relaxed. The clean surface contains a zigzag chain of alternating Ga and As atoms

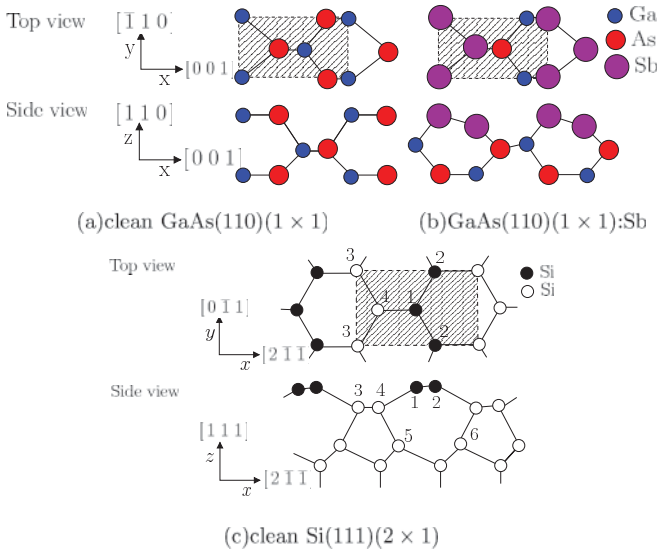

FIG. 1. (Color online) Top and side views of the (a) clean GaAs(110)(1 × 1) surface, (b) Sb-covered GaAs(110)(1 × 1) surface, and (c) clean Si(111)(2 × 1) surface. The coordinate axes for the GaAs(110)(1 × 1) surfaces are $x = [001]$, $y = [\bar{1}10]$, and $z = [110]$, and for the Si(111)(2 × 1) are $x = [2\bar{1}\,\bar{1}]$, $y = [0\bar{1}1]$, and $z = [111]$. The shaded area is the surface unit cell.

along the y direction $[\bar{1}10]$, which are replaced by Sb atoms in the Sb-covered surface. To better describe the surface states for the clean[36] and Sb-covered[37] surfaces, the scissors shift used is 1 eV for the clean surface and 0.8 eV for the Sb-terminated one.

Figure 2 demonstrates the photon energy dependence of $\tilde{\eta}^{yyx}(\ell = 1|0;\omega,-\omega)$ for the clean GaAs(110) surface, as calculated for two slabs, both of them have the upper part terminated by the structure of the clean GaAs(110). The first slab has a Sb-terminated back surface, while the second slab

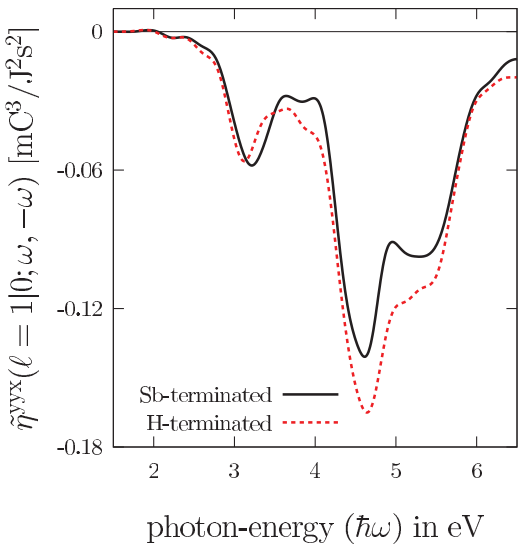

FIG. 2. (Color online) $\tilde{\eta}^{yyx}(\ell = 1|0;\omega,-\omega)$ vs. the photon energy for the clean GaAs(110)(1 × 1) surface. The solid line is for an slab with back-surface Sb-terminated, whereas the dotted line is for an slab with back-surface H-terminated. Here the number of layers $N_c = 25$.

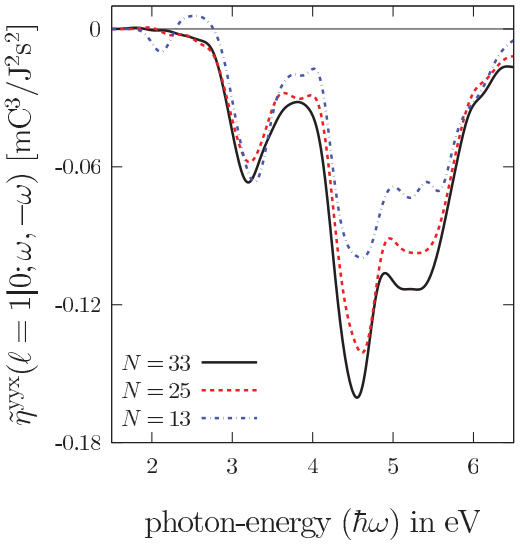

FIG. 3. (Color online) $\tilde{\eta}^{yyx}(\ell = 1|0;\omega,-\omega)$ vs. the photon energy for the clean GaAs(110)(1 × 1) surface and for different values of the number of layers N. The slab has its back-surface Sb terminated.

has H-terminated back surface. We have to stress that both results are very similar, clearly indicating that the layer-by-layer approach is able to correctly provide the same results for the front surface regardless of what the back-surface termination is. In Fig. 3 we show $\tilde{\eta}^{yyx}(\ell = 1|0;\omega,-\omega)$ vs. the photon energy for the clean GaAs(110) surface obtained from a slab with Sb-terminated back surface for $N = 13$, 25, and 33 layers. We notice that the injection current curves for 25 and 33 layers are rather similar and that the difference is more pronounced for the slab with 13 layers. This can be understood simply from the fact that a slab with 13 layers is not sufficiently thick to completely decouple the front surface from the back surface of the slab. Still, the slab with 13 layers produces reasonable results and it might be used to estimate the injection current if a bigger surface unit cell is required. We take $N_c = 33$ for the slab that represents both the clean and the Sb-covered GaAs(110) surfaces. We found that for both clean and adsorbate covered surfaces $\ell_{\text{eff}} = 5$ with is corresponding value of L_{eff} properly included in $\tilde{\eta}^{yyx}(\ell|0;\omega,-\omega)$.

Figure 4 shows $\eta^{yyx}(\ell_B|0;\omega,-\omega)$ for the layer at the middle, $\ell_B = 17$, for the GaAs(110) slab with $N_c = 33$ and the back surface terminated with Sb, and $\eta^{yyx}_{\text{bulk}}(0;\omega,-\omega)$ using only the two $\boldsymbol{\alpha}_s$ obtained for this surface that belongs to the space group Pm.[26,38] We remark that $\eta^{yyx}_{\text{bulk}}(0;\omega,-\omega)$ was calculated for a bulk unit cell without using the full set of $\boldsymbol{\alpha}_s$ that correspond to the $\bar{4}\bar{3}m$ (zincblende) symmetry of GaAs. The resemblance of both results is striking and proves the validity of the layer-by-layer approach also for the "bulk" layers of an slab. We have checked that the three layers next to ℓ_B in either direction toward the front or back surface are rather similar and, thus, Eq. (15) is a reasonable definition for the surface response.

In Fig. 5 we show the total surface response $\eta^{S,yyx}(0;\omega,-\omega)$ and its layer-by-layer components $\tilde{\eta}^{yyx}(\ell|0;\omega,-\omega)$ for the first three layers of both the clean and the Sb-covered GaAs(110)(1 × 1) surfaces. Notice a substantial sensitivity of the signal to the surface termination type as the spectra

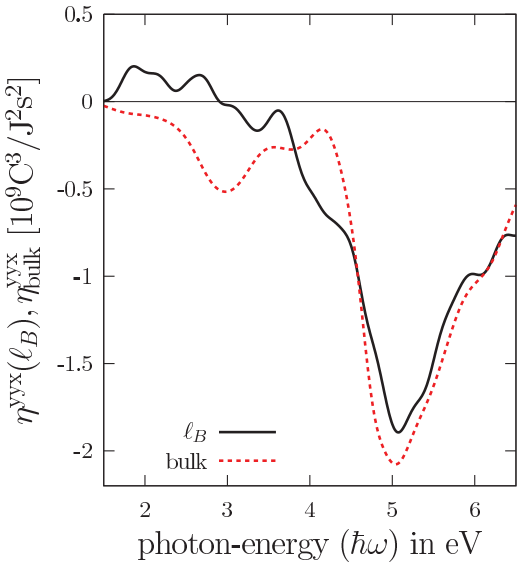

FIG. 4. (Color online) $\eta^{yyx}(\ell_B|0;\omega,-\omega)$ and $\eta^{yyx}_{\rm bulk}(0;\omega,-\omega)$ vs. the photon energy, see text for details.

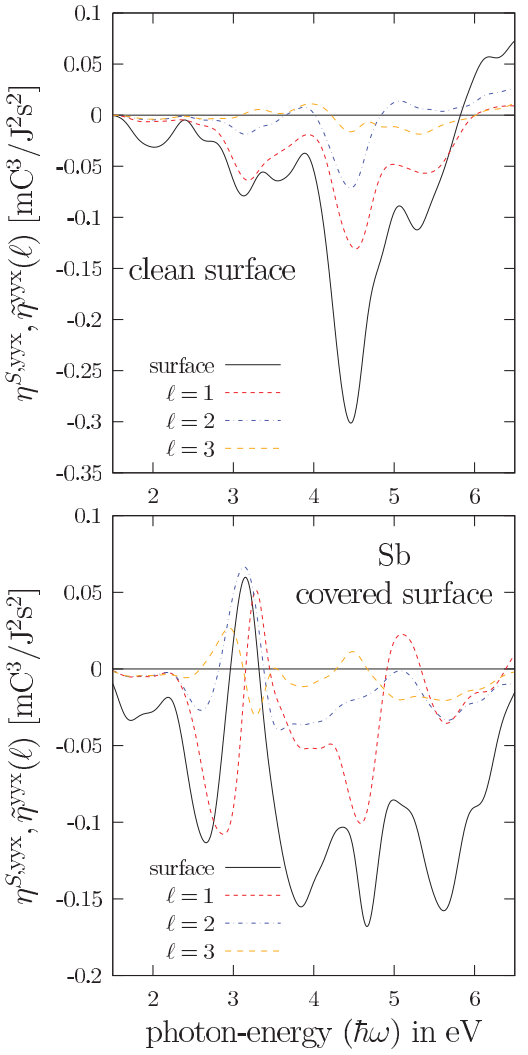

FIG. 5. (Color online) $\eta^{S,yyx}(0;\omega,-\omega)$ and $\tilde{\eta}^{yyx}(\ell|0;\omega,-\omega)$ for the clean (top panel) and one-monolayer Sb-covered (bottom panel) GaAs(110)(1 × 1) surfaces. $\ell = 1$ in the clean (Sb-covered) surface corresponds to the zigzag chains of Ga and As (Sb) atoms, and $\ell = 2,3$ corresponds to the second and third layer of Ga and As atoms for both surfaces.

are different in both cases, especially below 5 eV, the energy range that is easily accessible experimentally. The injection current for both surfaces are of the same order of magnitude and demonstrate distinctive spectral features. For instance, the strong dip at ∼4.3 eV for the clean surface originates from the well-known E_2 critical point (CP) of GaAs electronic band structure, and the small dip ∼3.1 eV can be associated to the E_1 CP. Of course these resonances are modified by the presence of the surface and adsorbate. Indeed, the Sb-covered surface demonstrates richer spectral features due to the surface- and bulk-surface-modified electronic states. For this Sb-modified GaAs(110), a dip-peak feature around 3 eV is related to the surface modified E_1 CP, and a dip around 4.6 eV can again be related to the surface modified E_2 CP. Likewise, the other structures could also be related to different CP (for instance, E_1' for the Sb-covered surface at ∼5.5 eV) or to the interference of several of these CP in combination with surface resonances. The layer-by-layer decomposition of the injection current signal also allows us to see how these resonances depend on the atomic layer of the surface. For the clean surface we see that the first layer of Ga and As atoms dominates the E_1 dip, whereas for the E_2 dip, there is also a contribution from the second layer and a smaller one from the third. For the Sb-covered GaAs(110), we see that the top Sb layer contribution to the injection current dominates, in particular, in the E_1 and E_2 spectral features, while only a small contribution comes from the first and second layer of Ga and As atoms. From Eq. (17) it follows that the injected current flows along the y direction; that is, excited electrons move along the zigzag chains of atoms. By changing the phase difference between two light polarizations we can efficiently control the current direction along the surface. As explained above, it is interesting to see how different spectral features of $\eta^{S,yyx}(0;\omega,-\omega)$ could be assigned to different layers. For instance, the negative peak at ∼3 eV in the clean surface essentially comes from the first layer of atoms, whereas the peak at ∼4.3 eV mainly comes from the first three atomic layers, with a larger contribution from the first layer, though. For the Sb-covered surface, the negative peak at ∼2.7 eV is dominated by the current along Sb zigzag chains that correspond to $\ell = 1$ in Fig. 5, and then the positive peak at 3.15 eV has contributions mainly from the first three layers. It is interesting that the antimony layer and second GaAs layer ($\ell = 3$) produce a current in the same negative y direction, whereas the contribution from the first GaAs layer ($\ell = 2$) points in the opposite direction. Above the 3.1 eV peak, the spectrum is partially dominated by the Sb layer, although there are clear contributions to the current from the first two GaAs layers. Finally, the layer-by-layer contribution for $\ell = 3$ is different for the clean and antimony-terminated surfaces despite similar neighboring layers ($\ell = 2$ and $\ell = 4$). It again demonstrates essential sensitivity of the surface injection current to even minor modification in the atomic positions.

B. Si(111) surfaces

Now we show the results for a clean cleaved Si(111) surface. This surface demonstrates a 2×1 Pandey reconstruction and is characterized by buckled zigzag chains along the y ($[01\bar{1}]$) direction.[15,39] The upper atoms, labeled 2 in Fig. 1, show sp^3-like electron configuration with one dangling bond predominantly filled, while the lower atoms labeled 1 exhibit sp^2-like bonding with their p_z dangling bond predominantly empty. As for the GaAs(110)(1×1) surfaces, the current moves along the zigzag chains of Si atoms along y. In Fig. 6, we show $\eta^{S,yyx}(0;\omega,-\omega)$ and $\tilde{\eta}^{yyx}(\ell|0;\omega,-\omega)$ vs. the photon energy for the clean Si(111) 2×1. The different values of ℓ correspond to the topmost atomic layer ($\ell = 1$) composed by the Si buckled chains, and the next two atomic layers ($\ell = 2,3$) of Si atoms. For this surface we used a slab that is H-terminated on its back with $N_c = 19$ layers, and a scissors shift of 0.43 eV was applied.[40] We see that the surface response, which dominates in the injection current, starts rising sharply around 0.5 eV, which corresponds to the transitions between the surface states, reaching its maximum at 0.75 eV and followed with a sharp decline. Above 4 eV the signal is basically zero. The calculated layer-by-layer responses, $\tilde{\eta}^{yyx}(\ell|0;\omega,-\omega)$, convincingly demonstrates that the surface signal is dominated by a contribution from the first two atomic layers and that after the third layer $\tilde{\eta}^{yyx}(\ell \geqslant 4|0;\omega,-\omega) \approx 0$ (not shown in the figure). Therefore, L_{eff} would correspond to the total thickness of the first 3 layers and $\ell_{\text{eff}} = 3$. Surprisingly, very few atomic layers beneath the Si(111)2×1 surface behave as noncentrosymmetric. After the fourth layer, the system can be treated as centrosymmetric as far as this response is concerned. As can be seen from Fig. 6, the corresponding surface injection current occurs below the direct bulk band gap of Si (approximately around 3 eV), this is because the prominent surface energy levels appear within the gap of the projected-bulk band structure. This was experimentally shown in Ref. 40 for the surface optical response of the Si(111)2×1 surface. In contrast to the GaAs(110) surfaces, we see that for Si(111)2×1, the surface electronic transitions dominate the injection current with almost no contribution from the surface-modified bulk transitions. Indeed, in Fig. 6 we see a very small spectral feature above 3 eV that is related to the E_1 CP of Si compared to transitions between the surface states due to the surface chains.

C. Surface vs. bulk experimental detection estimate

The detection of injection current usually requires measurements of voltage induced along the surface[7] or terahertz radiation generated by an incident optical pulse.[5,6] To demonstrate that the surface injection current effect is strong enough to be observed experimentally, we refer to the study of bulk injection current in hexagonal CdSe bulk by Laman *et al.*[7] There the current injection generation was restricted to the penetration depth $l \approx 1.8\,\mu$m of the incident radiation; therefore, the signal can be associated with an effective surface injection coefficient $\eta^S = l\eta^B$, where η^B is the bulk coefficient. The injection current was studied in the presence of carrier momentum relaxation time, $\tau \approx 40$ fs, resulting in $J_{\text{inj}} \propto 4\tau\eta^B|E_0|^2$ [see Eq. (17)], where an effective surface current $J^S_{\text{inj}} = lJ_{\text{inj}}$ of magnitude 5.4 nA/cm was detected,[7] corresponding to an effective surface injection coefficient $\eta^S = 90$ mC^3/(J^{2}s^2). This experimental value is larger than our calculated values by less than two orders of magnitude. However, the measurements of injection current in Ref. 7 were done at very low incident light intensity of only 0.06 W/cm^2. As seen from Eq. (17), the signal from these effects scales linearly with the incident intensity; thus, an easily observable signal from surface injection current should be possible at intensities low enough to avoid surface damage. Finally, the injection current periodic dependence on the phase shift between two perpendicular light polarizations provides a straightforward way to discriminate the injection current from various surface photovoltaic effects.

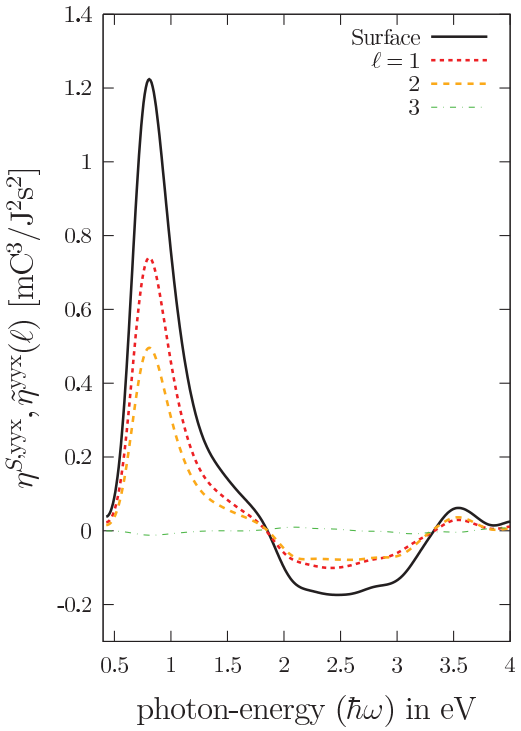

FIG. 6. (Color online) $\eta^{S,yyx}(0;\omega,-\omega)$ and $\tilde{\eta}^{yyx}(\ell|0;\omega,-\omega)$ for the clean reconstructed Si(111)(2×1) surface. $\ell = 1$ corresponds to the buckled zigzag chains of Si atoms.

V. CONCLUSIONS

We have developed a layer-by-layer formalism for the coherent control of the surface injection current. An efficient numerical approach to calculate the current at the surfaces of semiconductor crystals was proposed. The strong surface sensitivity of the injection current was clearly demonstrated: since the injection current is zero for crystals with bulk inversion symmetry or $\bar{6}m2$, $\bar{6}$, and $\bar{4}\bar{3}m$ (zincblende) symmetry, the experimental measurements of such a current present a valuable tool for noninvasive characterization of semiconductor surfaces. Following the layer-by-layer approach, we derived the macroscopic response tensor that describes the surface injection current. We performed *ab initio* calculations of the current to evaluate the response for a few prototypical surfaces such as the clean and Sb-terminated GaAs(110)(1×1) surfaces and the clean Si(111)(2×1) surface. The surface

injection current is found to be very sensitive to such important semiconductor surface parameters as reconstruction, adsorbates type, and bonding, which modify the electronic band structure. At all surfaces considered, contributions of the surface states are clearly present in the calculated spectra of the surface injection coefficients. The layer-by-layer analysis proved to be crucial in order to extract the response of each atomic layer of any given system and, thus, allows us to explain the surface behavior as the sum of the contributions of the different atomic planes.

Like other conventional optical techniques, injection current measurements requires a comparatively simple experimental setup. An attractive feature of the proposed effect is that the surface injection current involves real transitions rather than virtual transitions between electron bands where the system is left in the final excited state. This is in contrast, for instance, to SSHG, which is a parametric process and typically only probes virtual excitation to excited states. Since the nature of these initial and final excited states can be understood in terms of the symmetry and the structure of the surface, it is possible to interpret the injection current in a much more straightforward way than the signal due to SSHG. Comparing to RAS, which is not sensitive to highly symmetric surfaces, such as Si(111)(1 × 1)As or Si(111)7 × 7, the injection current exists for such or similar surfaces.[41] Another attractive feature of the effect is that the injection current is linear in the incident optical intensity, unlike the quadratic dependence of SSHG. Although detection by terahertz radiation requires short pulses, we note that electrode detection of the injection current has been shown to be possible even with CW radiation.[6]

Finally, numerical estimates indicate that the surface injection current should be readily measurable, thus, offering the possibility of using optical coherent control to manipulate the actual motion of the electron at the surface. This leads to the exciting possibility of catalyzing and controlling growth and chemical reactions at surfaces by optically controlling directed electron motion. Experiments to investigate the surface injection current are clearly warranted.

ACKNOWLEDGMENTS

We acknowledge very useful discussions with F. Nastos and J.E. Sipe. J.L.C. acknowledges partial support by CONACyT-México. B.S.M. acknowledges the National Science and Engineering Research Council of Canada and Photonics Research Ontario and the Department of Physics of the University of Toronto, for the support during a sabbatical year, and support by CONACYT 153930. A.I.S. acknowledges the National Science and Engineering Research Council of Canada (NSERC), Photonics Research Ontario the Shared Hierarchical Academic Research Computing Network (SHARCNET), and the Centro de Investigaciones en Óptica for support during a partial sabbatical visit.

[1] P. Weightman, D. Martin, R. Cole, and T. Farrell, Rep. Prog. Phys. **68**, 075318 (2005).

[2] W. Richter, *Reflectance Anisotropy Spectroscopy and other Anisotropy based Spectroscopies in* Highlights of Light Spectroscopy on Semiconductors, edited by A. D'Andrea, L. G. Quagliano, and S. Selci, (World Scientific, Singapore, 1996), p. 81.

[3] M. Downer, B. S. Mendoza, and V. Gavrilenko, Surf. Interface Anal. **31**, 966 (2001).

[4] D. Lim, M. C. Downer, J. G. Ekerdt, N. Arzate, B. S. Mendoza, V. I. Gavrilenko, and R. Q. Wu, Phys. Rev. Lett. **84**, 3406 (2000).

[5] N. Côté, N. Laman, and H. van Driel, Appl. Phys. Lett. **80**, 905 (2002).

[6] N. Côté, J. Fraser, M. DeCamp, P. Bucksbaum, and H. van Driel, Appl. Phys. Lett. **75**, 3959 (1999).

[7] N. Laman, A. Shkrebtii, J. Sipe, and H. van Driel, Appl. Phys. Lett. **75**, 2581 (1999).

[8] F. Nastos, B. Olejnik, K. Schwarz, and J. E. Sipe, Phys. Rev. B **72**, 045223 (2005).

[9] J. E. Sipe and A. I. Shkrebtii, Phys. Rev. B **61**, 5337 (2000).

[10] For a recent use of the shift current to control GaAs interface, see G. C. Loata, M. Bieler, G. Hein, and U. Siegner, J. Opt. Soc. Am. B **25**, 1261 (2008).

[11] P. J. Sturman, *Photovoltaic and Photo-refractive Effects in Noncentrosymmetric Materials* (CRC, Boca Raton, 1992).

[12] C. Aversa and J. E. Sipe, IEEE J. Quantum Electron. **32**, 1570 (1996).

[13] C. Aversa and J. E. Sipe, Phys. Rev. B **52**, 14636 (1995).

[14] For example, in the CW limit $J^a_{\rm shift} \propto \cos(\phi_b - \phi_c)$ while $dJ^a_{\rm inj}/dt \propto \sin(\phi_b - \phi_c)$, where $E^{b,c}(\omega) = E^{b,c}(\omega)e^{i\phi_{b,c}}$, see Ref. 8.

[15] M. Rohlfing and S. Louie, Phys. Status Solidi A **175**, 17 (1999).

[16] S. Selci, F. Ciccacci, A. Cricenti, A. C. Felici, C. Goletti, and P. Chiaradia, Solid State Commun. **62**, 833 (1987).

[17] B. S. Mendoza, N. Arzate, and R. Vázquez-Nava, Phys. Status Solidi C **5**, 075318 (2008).

[18] The vacuum size, which we used, is sufficient to effectively decouple the surfaces of neighboring slabs in the supercells. For details, see Ref. 21, where the effect of the vacuum size on the optical response was studied in detail. Therefore, we can safely neglect a possible spurious interaction through tunneling of the wave functions from one surface to another and, consequently, consider each supercell as well isolated.

[19] C. Hogan, R. Del Sole, and G. Onida, Phys. Rev. B **68**, 035405 (2003).

[20] C. Castillo, B. S. Mendoza, W. G. Schmidt, P. H. Hahn, and F. Bechstedt, Phys. Rev. B **68**, 041310 (2003).

[21] B. S. Mendoza, F. Nastos, N. Arzate, and J. E. Sipe, Phys. Rev. B **74**, 075318 (2006).

[22] J. Mejía, C. Salazar, and B. Mendoza, Revista Mexicana de Fisica **50**, 134 (2004).

[23] J. Sipe, A. Shkrebtii, and O. Pulci, Phys. Status Solidi A **170**, 431 (1998).

[24] F. Nastos, J. Rioux, M. Strimas-Mackey, B. S. Mendoza, and J. E. Sipe, Phys. Rev. B **76**, 205113 (2007).

[25] Choosing inappropriate values for L_v leads to spurious results as analyzed in Ref. 21 for the linear optical response.

[26]X. Gonze, *et al.* Comput. Mater. Sci. **25**, 478 (2002).
[27]C. Hartwigsen, S. Goedecker, and J. Hutter, Phys. Rev. B **58**, 3641 (1998).
[28]S. Goedecker, M. Teter, and J. Hutter, Phys. Rev. B **54**, 1703 (1996).
[29]Z. H. Levine and D. C. Allan, Phys. Rev. B **44**, 12781 (1991).
[30]O. Pulci, G. Onida, R. Del Sole, and L. Reining, Phys. Rev. Lett. **81**, 5374 (1998).
[31]M. Rohlfing and S. G. Louie, Phys. Rev. Lett. **83**, 856 (1999).
[32]R. Del Sole and R. Girlanda, Phys. Rev. B **48**, 11789 (1993).
[33]H. Hübener, E. Luppi, and V. Véniard, Phys. Rev. B **83**, 115205 (2011).
[34]J. L. Cabellos, B. S. Mendoza, M. A. Escobar, F. Nastos, and J. E. Sipe, Phys. Rev. B **80**, 155205 (2009).
[35]For homopolar Si surfaces and nonpolar GaAs(110) surfaces there is no need to consider partially charged hydrogen, as required, for instance, in the case of GaAs(100) surfaces. Thus, for the structure optimization, the hydrogen layer at the back of the slab was attached to an ideal bulk-terminated surface and then relaxed, keeping the neighboring semiconductor atoms fixed.
[36]B. S. Mendoza, N. Esser, and W. Richter, Phys. Rev. B **67**, 165319 (2003).
[37]N. Esser, R. Hunger, J. Runberg, W. Richter, R. D. Sole, and A. I. Shkrebtii, Surf. Sci. **307–309**, 1045 (1994).
[38]See Bilbao crystallographic server [http://www.cryst.ehu.es].
[39]K. C. Pandey, Phys. Rev. Lett. **49**, 223 (1982).
[40]G. Chiarotti, S. Nannarone, R. Pastore, and P. Chiaradia, Phys. Rev. B **4**, 3398 (1971).
[41]B. Mendoza and J. L. Cabellos (private communication).